A

| Peptidergic Nociceptors (CGRP+) | Small (<20 pF) | Medium (20~30 pF) | Large (30~60 pF) |
|---|---|---|---|
| Nonrepeptitive Firing I<br>1-2 spikes at the onset | 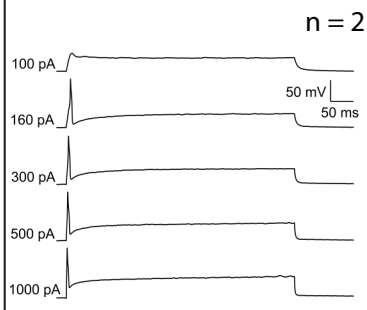 | 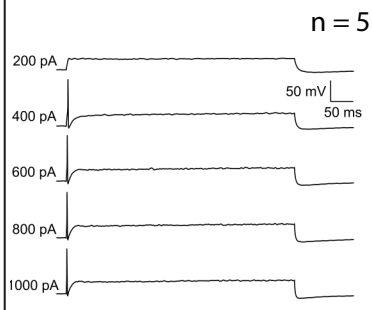 | 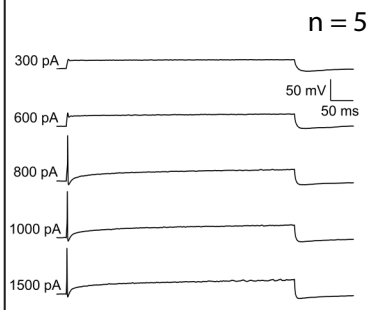 |
| Non-Repetitive Firing II<br>2-3 spikes | 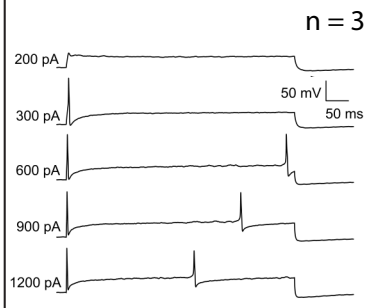 | 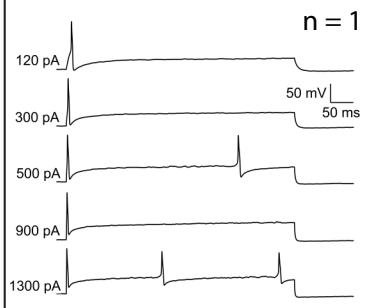 | |
| Repetitive Firing<br>> 3 spikes | 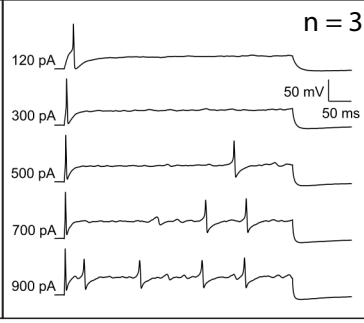 | 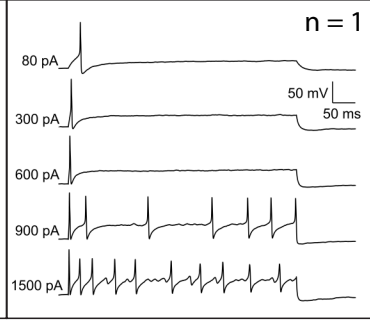 | |

B

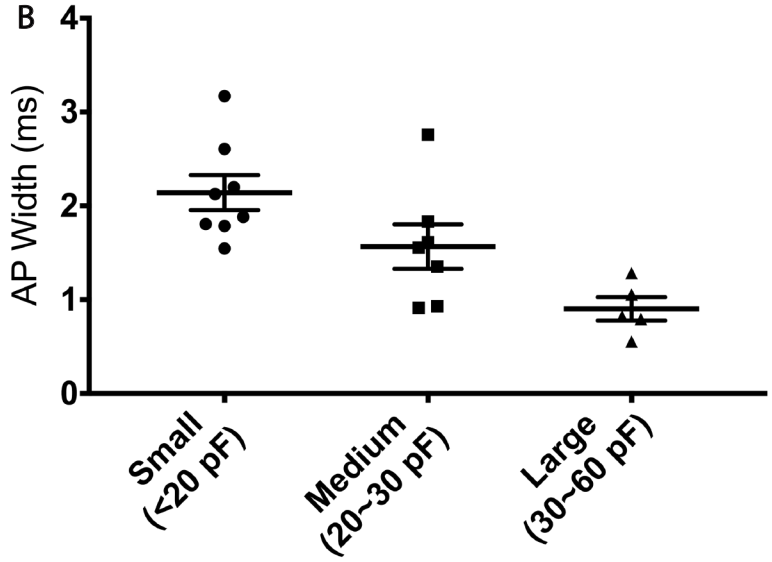

**Figure S1. Heterogeneity of intrinsic electrical properties of peptidergic nociceptors, Related to Figure 1**

(**A**) Representative *in vitro* spiking patterns of $CGRP^+$ peptidergic nociceptors evoked by 500-ms depolarizing current injections. $CGRP^+$ peptidergic nociceptors are categorized by membrane capacitance (horizontal) and spiking patterns (vertical). The number of observations in each category is noted on the top-right corner of each cell.

(**B**) AP widths of $CGRP^+$ peptidergic nociceptors categorized based on membrane capacitance as in (**A**) (total number of neurons =20).

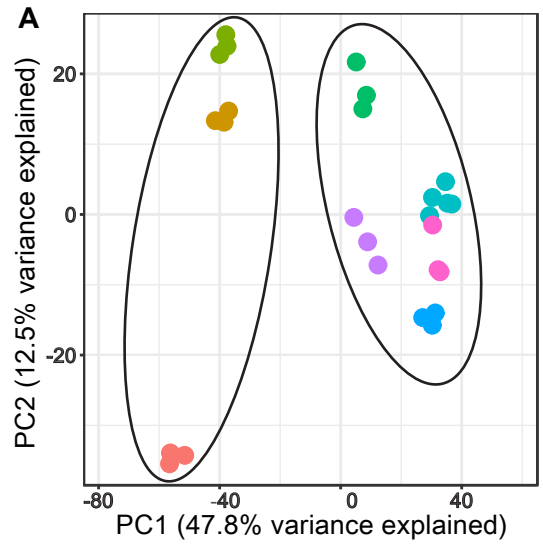


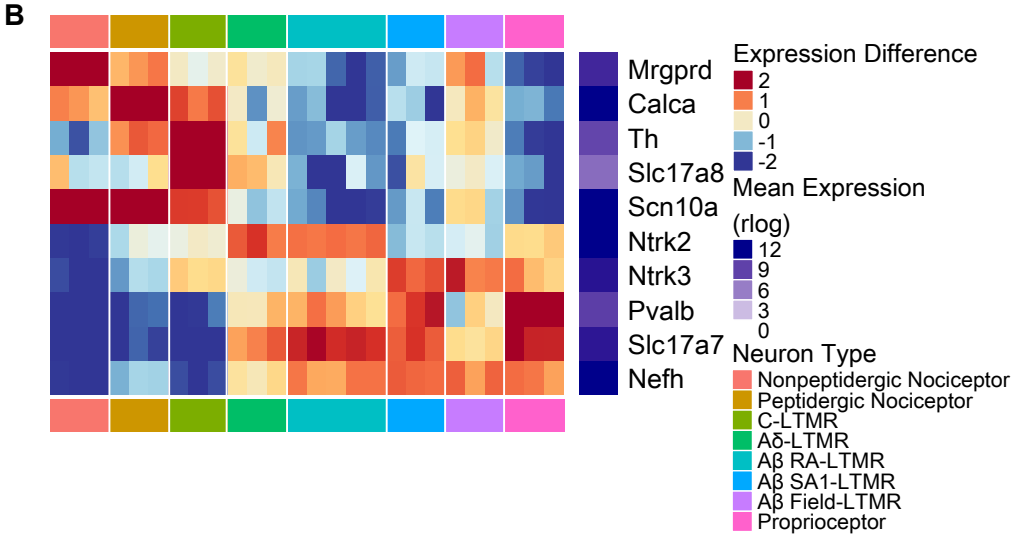


*Calb1*$^{dgCre}$;*Avil*$^{FlpO}$;*R26*$^{LSL\text{-}FSF\text{-}tdTomato}$ TMP100 µg/g x 2 days (P18,19)

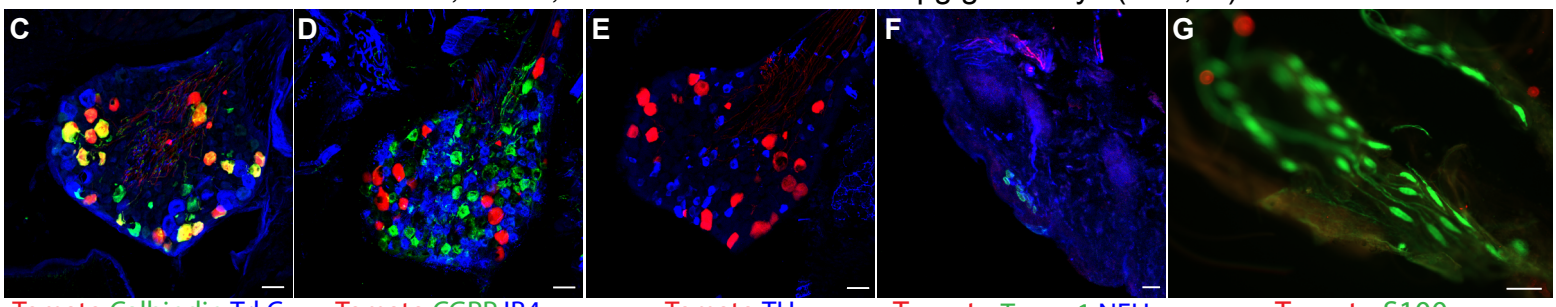


Tomato;Calbindin;TrkC | Tomato;CGRP;IB4 | Tomato;TH | Tomato;Troma1;NFH | Tomato;S100

*Calb1*$^{dgCre}$;*R26*$^{LSL\text{-}tdTomato}$;*TrkB*$^{GFP}$
TMP100 µg/g x 2 days (P18,19)

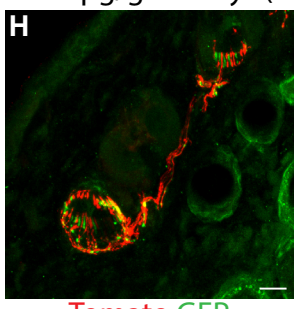


Tomato;GFP

*Calb1*$^{dgCre}$;*Brn3a*$^{AP}$
TMP100 µg/g x 2 days (P18,19)

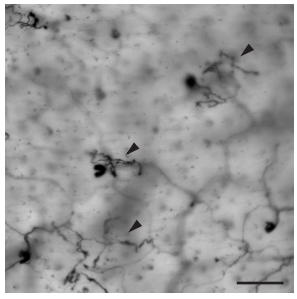


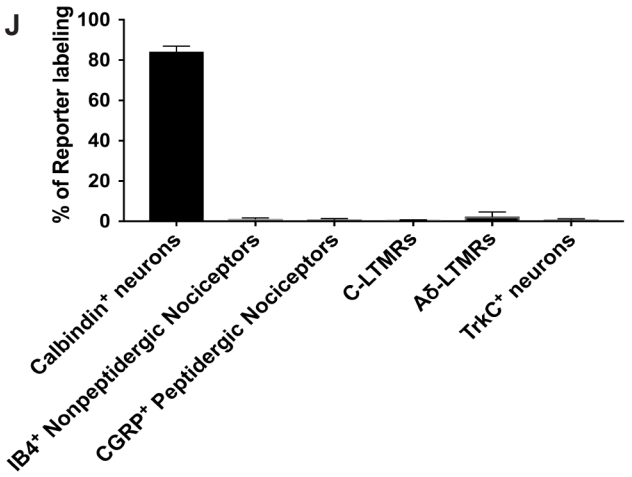

**Figure S2. Verification of transcriptome profiles, Related to Figure 2**

(**A**) Principal component analysis (PCA) of samples showing 1) most samples for the same neuronal subtype cluster with each other, and 2) two major clusters exist, MrgD$^{+}$ nonpeptidergic nociceptors, CGRP$^{+}$ peptidergic nociceptors and C-LTMRs as one cluster, Aδ-LTMRs, three Aβ-LTMR subtypes and proprioceptors as the other cluster, as shown in Figure 2C. The PCA analysis is based on the expression of the top 1000 genes that display the highest expression variance across samples. The two major cluster patterns are consistent using PCA analysis on expression of all genes or hierarchical clustering with expression of all genes. Expression levels are reported using rlog transformed count values.

(**B**) Heatmap depicting expression patterns across subtypes (columns) of marker genes (rows), including genes used for generating mouse tools that are employed in this study for subtype-specific labeling (Mrgprd (MrgD), Calca (CGRP), Th (TH), Ntrk2 (TrkB), Ntrk3 (TrkC), Pvalb (PV)) and genes of which the expression patterns have been previously studied (Slc17a8 (vGlut3), Scn10a (Nav1.8), Slc17a7 (vGlut1), Nefh (NFH)). Npy2r-GFP mice used to label Aβ RA-LTMRs is a BAC transgenic mouse line, and GFP expression does not recapitulate endogenous Npy2r gene expression, therefore Npy2r gene is not included here. Plotting scheme is the same as Figure 2D. See Star Methods for further details.

(**C**-**G**) Characterization of the *Calb1*$^{dgCre}$ mouse line.

(**C**-**E**) DRG sections from *Calb1*$^{dgCre}$*; Advillin*$^{FlpO}$*; R26*$^{LSL\text{-}FSF\text{-}tdTomato}$ (*Ai65*) mice treated with trimethoprim (TMP) show that the majority tdTomato+ neurons express Calbindin (84.2±2.8%, n=4 mice), but do not express markers of other sensory neuron subtypes,

IB4 (1.18±0.5%, n=4 mice), CGRP (0.93±0.4%, n=4 mice), TH (0.4±0.4%, n=4 mice), TrkC (0.9±0.3%, n=4 mice).

(**F**) An example of skin sections showing that tdTomato$^+$ endings are not associated with Merkel cells (n>200 clusters of Merkel cells and Aβ SA1-LTMRs from n=3 mice are examined).

(**G**) An example of whole mount staining of periosteum membrane showing that tdTomato$^+$ endings are not associated with Pacinian corpuscles (8 periosteum membranes of 8 different legs from n=4 mice are examined).

(**H**) An example of skin sections from *Calb1$^{dgCre}$; R26$^{LSL\text{-}tdTomato}$; TrkB$^{GFP}$* showing that tdTomato$^+$ endings are GFP$^-$ lanceolate endings (< 3%, n=3 mice), and are therefore not Aδ-LTMRs.

(**I**) An example of whole mount back hairy skin staining from a *Calb1$^{dgCre}$; Brn3a$^{f(AP)}$* animal showing that the majority of AP$^+$ endings are lanceolate endings, though occasionally AP$^+$ free nerve endings were seen (arrow heads).

(**J**) Percentage of tdTomato$^+$ DRG neurons or endings that express other molecular markers, as shown in (**C**-**G**). Data are represented using mean and SEM.

Scale bars, (**C**-**E**) 50um, (**G, I**) 200um, (**F**, **H**) 20um. See Star Methods for further details, including information regarding baseline activity and variability across litters.

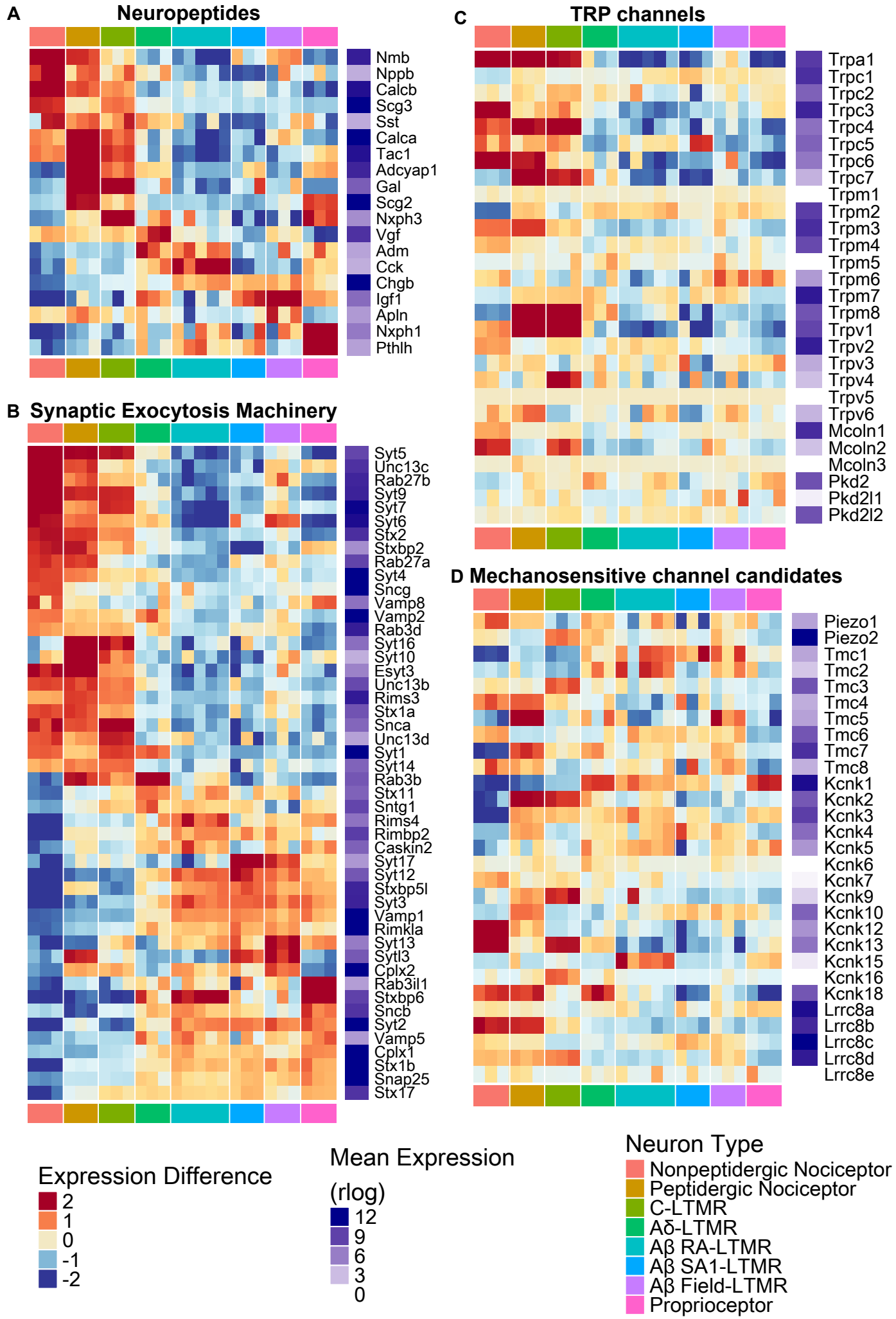
A
Neuropeptides
Nmb
Nppb
Calcb
Scg3
Sst
Calca
Tac1
Adcyap1
Gal
Scg2
Nxph3
Vgf
Adm
Cck
Chgb
Igf1
Apln
Nxph1
Pthlh
B
Synaptic Exocytosis Machinery
Syt5
Unc13c
Rab27b
Syt9
Syt7
Syt6
Stx2
Stxbp2
Rab27a
Syt4
Sncg
Vamp8
Vamp2
Rab3d
Syt16
Syt10
Esyt3
Unc13b
Rims3
Stx1a
Snca
Unc13d
Syt1
Syt14
Rab3b
Stx11
Sntg1
Rims4
Rimbp2
Caskin2
Syt17
Syt12
Stxbp5l
Syt3
Vamp1
Rimkla
Syt13
Sytl3
Cplx2
Rab3il1
Stxbp6
Sncb
Syt2
Vamp5
Cplx1
Stx1b
Snap25
Stx17
C
TRP channels
Trpa1
Trpc1
Trpc2
Trpc3
Trpc4
Trpc5
Trpc6
Trpc7
Trpm1
Trpm2
Trpm3
Trpm4
Trpm5
Trpm6
Trpm7
Trpm8
Trpv1
Trpv2
Trpv3
Trpv4
Trpv5
Trpv6
Mcoln1
Mcoln2
Mcoln3
Pkd2
Pkd2l1
Pkd2l2
D
Mechanosensitive channel candidates
Piezo1
Piezo2
Tmc1
Tmc2
Tmc3
Tmc4
Tmc5
Tmc6
Tmc7
Tmc8
Kcnk1
Kcnk2
Kcnk3
Kcnk4
Kcnk5
Kcnk6
Kcnk7
Kcnk9
Kcnk10
Kcnk12
Kcnk13
Kcnk15
Kcnk16
Kcnk18
Lrrc8a
Lrrc8b
Lrrc8c
Lrrc8d
Lrrc8e
Expression Difference
2
1
0
-1
-2
Mean Expression
(rlog)
12
9
6
3
0
Neuron Type
Nonpeptidergic Nociceptor
Peptidergic Nociceptor
C-LTMR
Aδ-LTMR
Aβ RA-LTMR
Aβ SA1-LTMR
Aβ Field-LTMR
Proprioceptor

**Figure S3. Expression patterns of genes grouped by functional categories, Related to Figure 3 and 4**

(**A**-**D**) Heatmap depicting expression patterns of genes encoding neuropeptides (**A**), synaptic exocytosis machinery proteins (**B**), TRP channels (**C**), and channels implicated in mechanosensation (**D**). For **A** and **B**, only genes that are both highly expressed and highly variable were selected for plotting, same as in Figure 3. For **C** and **D**, all genes were included and are arranged in alphabetical order, otherwise the plotting scheme was the same as Figure 2C and other heatmaps.

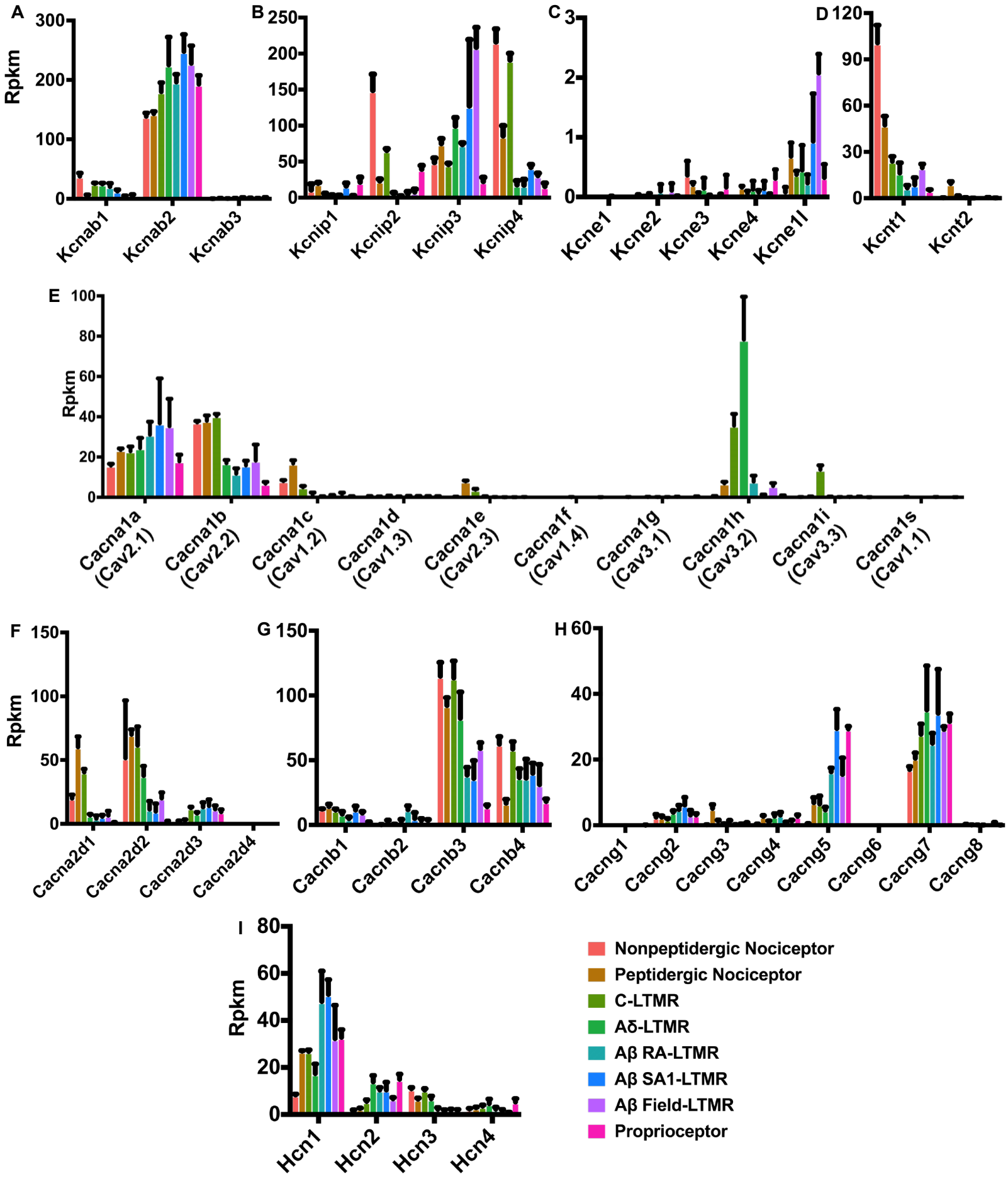
A
Rpkm
300
200
100
0
Kcnab1
Kcnab2
Kcnab3
B
250
200
150
100
50
0
Kcnip1
Kcnip2
Kcnip3
Kcnip4
C
3
2
1
0
Kcne1
Kcne2
Kcne3
Kcne4
Kcne1l
D
120
90
60
30
0
Kcnt1
Kcnt2
E
Rpkm
100
80
60
40
20
0
Cacna1a (Cav2.1)
Cacna1b (Cav2.2)
Cacna1c (Cav1.2)
Cacna1d (Cav1.3)
Cacna1e (Cav2.3)
Cacna1f (Cav1.4)
Cacna1g (Cav3.1)
Cacna1h (Cav3.2)
Cacna1i (Cav3.3)
Cacna1s (Cav1.1)
F
Rpkm
150
100
50
0
Cacna2d1
Cacna2d2
Cacna2d3
Cacna2d4
G
150
100
50
0
Cacnb1
Cacnb2
Cacnb3
Cacnb4
H
60
40
20
0
Cacng1
Cacng2
Cacng3
Cacng4
Cacng5
Cacng6
Cacng7
Cacng8
I
Rpkm
80
60
40
20
0
Hcn1
Hcn2
Hcn3
Hcn4
Nonpeptidergic Nociceptor
Peptidergic Nociceptor
C-LTMR
Aδ-LTMR
Aβ RA-LTMR
Aβ SA1-LTMR
Aβ Field-LTMR
Proprioceptor

**Figure S4. Expression patterns of genes encoding voltage-gated ion channels, Related to Figure 4**

(**A**-**E**) Bar plots showing expression levels of genes encoding Kv channel subfamily A member regulatory β subunits (**A**), Kv channel-interacting proteins (KCNIPs) (**B**), Kv channel subfamily E regulatory β subunits (**C**), sodium-activated potassium channel subfamily T subunits (**D**), Cav channels $\alpha_1$ subunits (**E**), $\alpha_2\delta$ subunits (**F**), β subunits (**G**) and γ subunits (**H**), and HCN channels (**I**). Expression levels were reported using rpkm values, and mean ± SD are shown using error bars.

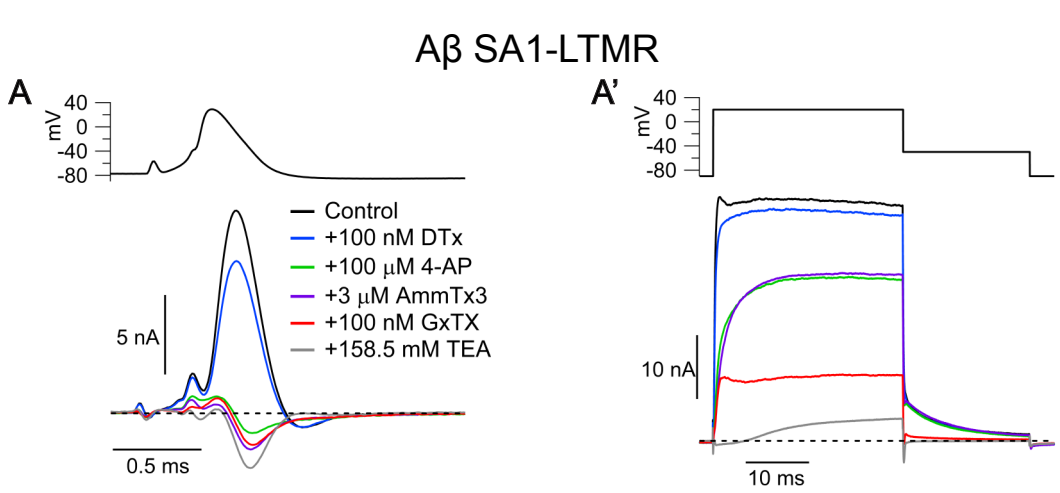


B

| Agent | Target | $IC_{50}$ | Test Concentration |
|---|---|---|---|
| α-Dendrotoxin (DTx) | Kv1.1, Kv1.2, Kv1.6 | 20 nM | 100 nM |
| 4-aminopyridine (4-AP) | Kv3 | 30 μM | 100 μM |
| AmmTx3 | Kv4.2, Kv4.3 | 100 nM | 3 μM |
| Guangxitoxin-1E (GxTX) | Kv2.1, Kv2.2 | 5 nM | 100 nM |

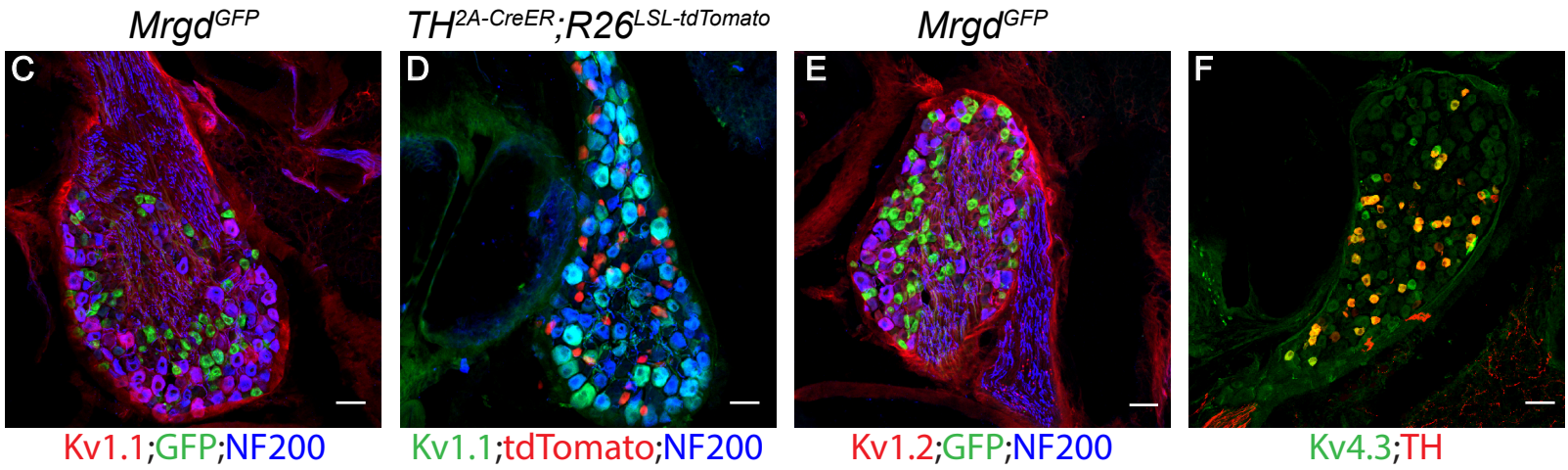

**Figure S5. Strategy for pharmacological dissection of potassium current and immunocytochemical characterization of expression of Kv1.1, Kv1.2 and Kv4.3 in distinct DRG subtypes, Related to Figure 5**

(**A**, **A'**) Outward current in an Aβ SA1-LTMR neuron during cumulative stepwise applications of a series of Kv channel inhibitors (in the continuous presence of 1 μM tetrodotoxin (TTX) and 1 μM A-803467 to inhibit inward current from Nav channels). Current was evoked by both an AP waveform command (**A**) and a step depolarization to +20 mV (**A'**) without Kv channel inhibitors (black) and cumulative application of 100 nM α-DTX (blue trace), 100 μM 4-AP (green), 3 μM AmmTx3 (purple), Guangxitoxin-1E (red) and 158.5 mM TEA (replacing sodium and potassium in the external solution, with all other blockers also present, grey). The sequence and concentrations of inhibitors were designed to define Kv1, Kv3, Kv4, and Kv2 components of current, with addition of high TEA to block any remaining potassium current and thereby define total potassium current.

(**B**) Table of potassium channel inhibitors applied in sequence with their expected channel targets and corresponding concentrations used in (**A**-**A'**) and Figure 5. At 100 μM, 4-AP can inhibit both Kv1 and Kv3 channels, but in all the DRG neuron subtypes, Kv1 expression is limited to Kv1.1, Kv1.2, and Kv1.6 subunits, all of which should be blocked by the preceding exposure to α-DTX.

(**C**-**D**) Representative images of immunolabeled DRG sections showing that Kv1.1 expression largely overlaps with NFH expression, but not with fluorescent reporters that label MrgD$^{+}$ nonpeptidergic nociceptors (**C**) or C-LTMRs (**D**).

(**E**) Representative images of immunolabeled DRG sections showing that Kv1.2 expression largely overlaps with NFH expression, but not with fluorescent reporters that label MrgD$^{+}$ nonpeptidergic nociceptors.

(**F**) Representative images of immunolabeled DRG sections showing that Kv4.3 expression largely overlaps with TH expression (Kv4.3 and TH$^{+}$/TH$^{+}$, 83±3%; Kv4.3 and TH$^{+}$/Kv4.3$^{+}$, 71±5%; n=3 mice). Data are represented using mean and SEM.

For (**C**-**F**), Scale bars, 50µm.

## Nonpeptidergic nociceptor

A

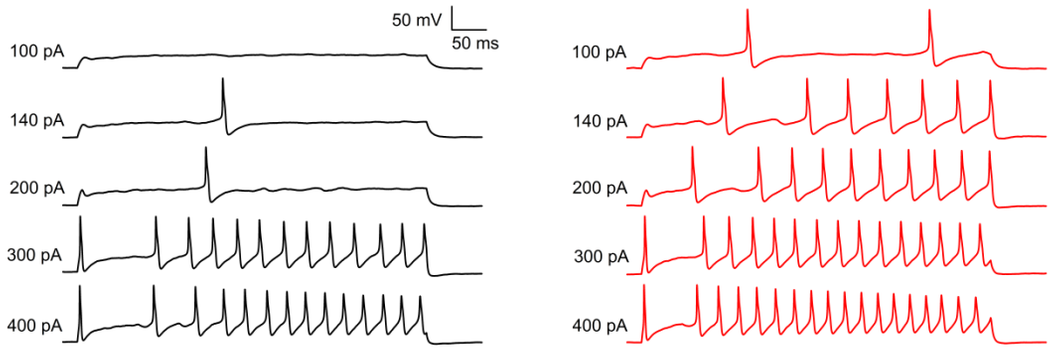


B

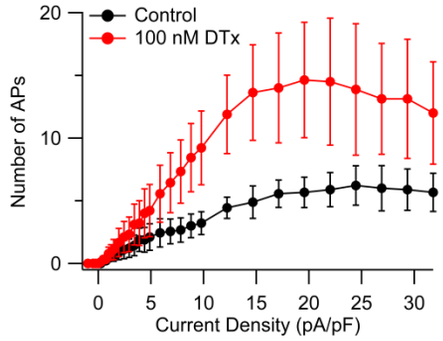


## C-LTMR

C

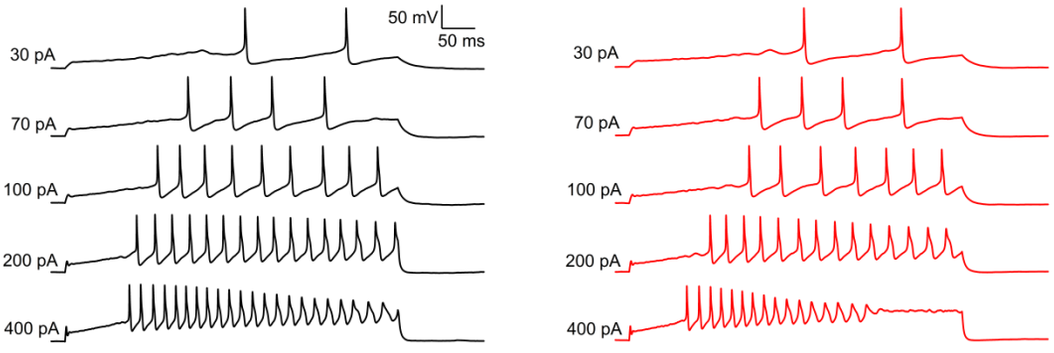


D

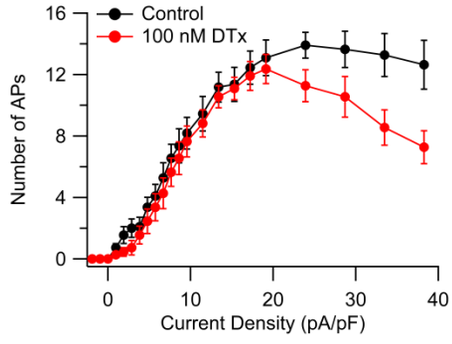

**Figure S6. Differing effects of blocking Kv1 channels on firing patterns of MrgD$^+$ nonpeptidergic nociceptors and C-LTMRs, Related to Figure 6.**

(**A, C**) Representative voltage traces showing the spike patterns of a MrgD$^+$ nonpeptidergic nociceptor (**A**) and a C-LTMR (**C**) during 500-ms current injections before and after application of 100 nM α-DTX.

(**B, D**) Number of APs during 500-ms current injections as a function of injected current density before (black circles) and after (red circles) α-DTX for MrgD$^+$ nonpeptidergic nociceptors (**B**, n=9) and C-LTMRs (**D**, n=11). Data are represented as mean ± SEM.

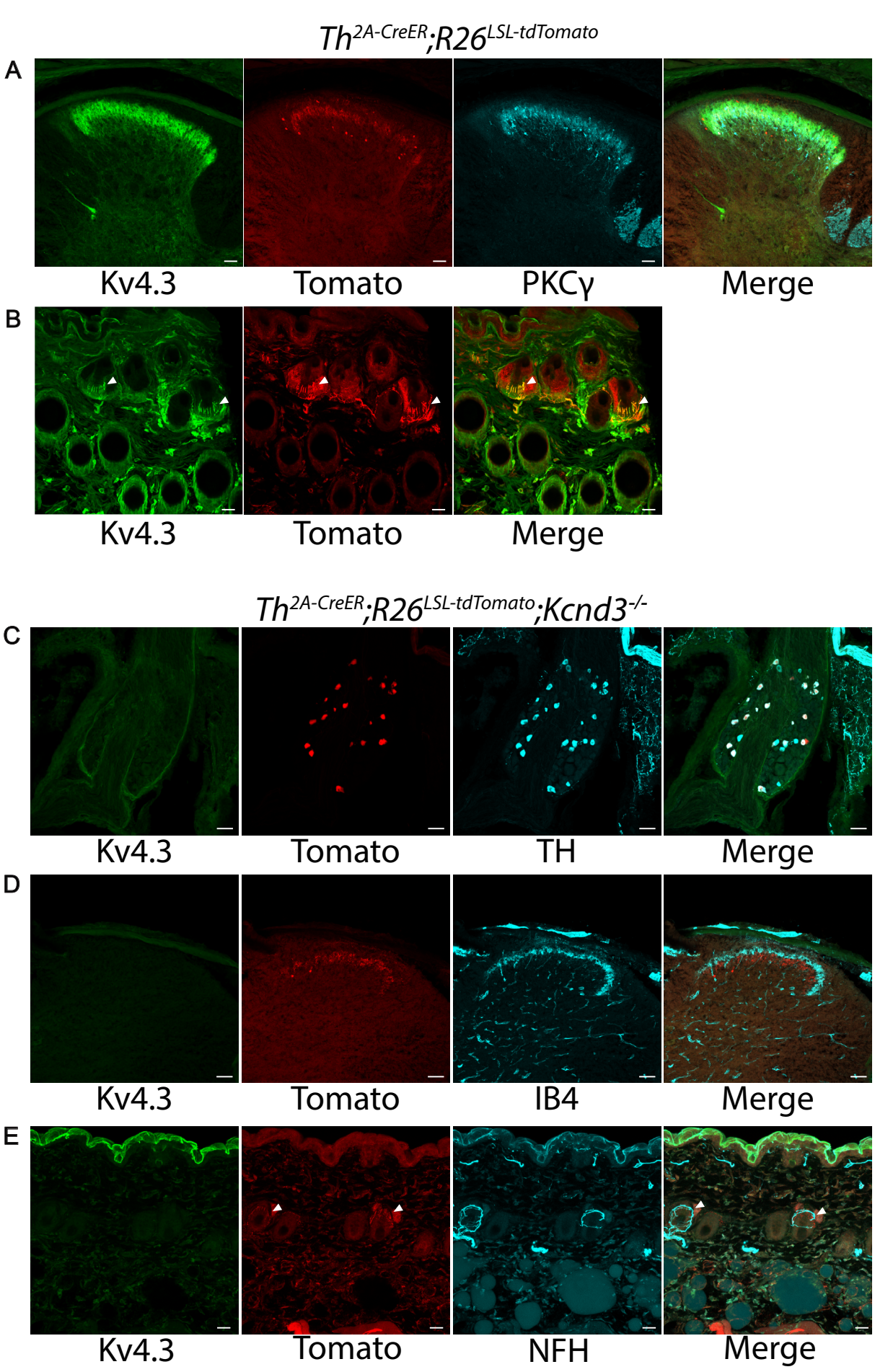
Th2A-CreER;R26LSL-tdTomato
A
Kv4.3
Tomato
PKCγ
Merge
B
Kv4.3
Tomato
Merge
Th2A-CreER;R26LSL-tdTomato;Kcnd3-/-
C
Kv4.3
Tomato
TH
Merge
D
Kv4.3
Tomato
IB4
Merge
E
Kv4.3
Tomato
NFH
Merge

**Figure S7. Kv4.3 is expressed in both C-LTMR cell bodies and axons and its genetic deletion does not change the general morphology of C-LTMRs, Related to Figure 7**

(**A**) Representative images of triple-immunostaining with Kv4.3, tdTomato, and PKCγ antibodies in cross sections of spinal cords from *Th$^{2A\text{-}CreER}$; R26$^{lsl\text{-}tdTomato}$(Ai14)* mice (TAM 2mg/day at P21-22). Each channel and merged channels are shown in individual panels. The merged channel image shows that Kv4.3 expression in the spinal cord dorsal horn largely overlaps with tdTomato and PKCγ.

(**B**) Representative images of double-immunostaining with Kv4.3 and tdTomato antibodies in back hairy skin sections from *Th$^{2A\text{-}CreER}$; R26$^{lsl\text{-}tdTomato}$(Ai14)* mice (TAM 2mg/day at P21-22). The merged image shows that Kv4.3 is present in C-LTMR hair follicle lanceolate endings marked by tdTomato.

(**C**) Representative images of triple-immunostaining with Kv4.3, tdTomato, and TH antibodies in DRG sections from *Th$^{2A\text{-}CreER}$; R26$^{lsl\text{-}tdTomato}$*; *Kcnd3$^{-/-}$* mice (TAM 2mg/day at P21-22). Immunostaining shows no Kv4.3 signal in DRGs of *Kcnd3-/-* mice, verifying the specificity of the Kv4.3 antibody.

(**D**) Representative images of triple-immunostaining with Kv4.3, tdTomato, and IB4 in cross sections of spinal cords from *Th$^{2A\text{-}CreER}$; R26$^{lsl\text{-}tdTomato}$(Ai14); Kcnd3$^{-/-}$* mice (TAM 2mg/day at P21-22). Kv4.3 signal is undetectable in spinal cords of *Kcnd3-/-* mice. TdTomato signal in C-LTMR central terminals is largely restricted to the region immediately ventral to the IB4 layer of the spinal cord dorsal horn, as in WT mice.

(**E**) Representative images of triple-immunostaining with Kv4.3, tdTomato, and NFH in back hairy skin sections from *Th$^{2A\text{-}CreER}$; R26$^{lsl\text{-}tdTomato}$(Ai14)*; *Kcnd3$^{-/-}$* mice (TAM

2mg/day at P21-22). No Kv4.3 signal is detected in the skin of *Kcnd3*$^{-/-}$ mice. TdTomato signal is present in lanceolate endings in these mutants, as it is in control mice.

For each staining experiment, n = 3 mice. For **A**, **C**, **D**, scale bars, 50µm; for **B**, **E**, scale bars, 20µm.

| | Nav1.1 | | Nav1.6 | | Nav1.7 | | Nav1.8 | | Kv1 | Kv2 | Kv3 | Kv4 | |
|---|---|---|---|---|---|---|---|---|---|---|---|---|---|
| | m | h | m | h | m | h | m | h | m | m | m | m | h |
| p | 3 | 1 | 3 | 1 | 3 | 1 | 2 | 1 | 4 | 4 | 4 | 4 | 1 |
| Vh | -35 | -40 | -39 | -53 | -18 | -40 | -11 | -32.4 | -57 | -32 | -15 | -50 | -73 |
| k | 5.5 | 12 | 5.5 | 5.4 | 7 | 12 | 3.8 | 6.1 | 11 | 8.6 | 8 | 17.6 | 4 |
| aL | 0.006 | 1.98 | 0.006 | 0.7 | 0.006 | 1.98 | 0.2 | 0.31 | 0 | 15 | 1 | 0.6 | 24.2 |
| bL | 0.08 | 8.54 | 0.08 | 8.5 | 0.08 | 8.54 | 0.4 | 42 | 4.59 | 53.1 | 15 | 1.5 | 191.9 |
| cL | -55 | -73.3 | -55 | -60.1 | -55 | -73.3 | -44.2 | -18.5 | -56 | -46.3 | -50 | -87 | 79.1 |
| dL | 12 | 4.7 | 12 | 8.4 | 12 | 4.7 | 8.02 | 11.1 | 15.4 | 14 | 10 | 6.16 | 4.67 |
| VBrk | -50 | -55 | -50 | -50 | -50 | -55 | -30 | -30 | -60 | -30 | -20 | -70 | -78 |
| aR | 0.015 | 0.17 | 0.015 | 0.1 | 0.015 | 0.17 | 0.36 | 0.3 | 0.21 | 0.75 | 0.15 | 0.5 | 22.5 |
| bR | 0.065 | 10.82 | 0.065 | 52.2 | 0.065 | 10.82 | 6 | 282 | 5.6 | 23 | 10 | 1.5 | 211.5 |
| cR | -10.8 | -39.1 | -10.8 | -59.5 | -10.8 | -39.1 | -39.6 | -55.8 | -96 | -25.6 | -10 | -50.5 | -66.3 |
| dR | 10 | 4.59 | 10 | 5 | 10 | 4.59 | 6.42 | 10 | 19.6 | 4.6 | 6 | 11.8 | 5.59 |
| Vrev(mV) | 55 | | | | | | | | -88 | | | | |
| $\bar{g}$ AβSA1 (mS/cm$^2$) | 8 | | 40 | | 5 | | 0 | | 6 | 12 | 4 | 0.8 | |
| $\bar{g}$ CLTMR (mS/cm$^2$) | 0 | | 0 | | 30 | | 40 | | 0.6 | 2 | 0.5 | 11 | |

**Table S1. Equations and parameters for voltage-gated ion channels in the computational model, Related to Figure 8**

The probability of a channel being open is described by the Hodgkin-Huxley-style parameters m (governing activation) and h (governing inactivation), each varying between 0 and 1 in a voltage- and time-dependent manner, with p being an exponent varying from 1 to 4. Steady-state voltage-dependence of m is given by $m_\infty = \frac{1}{1+\exp\left(\frac{-(V-Vh)}{k}\right)}$, where Vh is the voltage at which m is 0.5 and k is the slope factor. Steady-state voltage-dependence of h is given by $h_\infty = \frac{1}{1+\exp\left(\frac{V-Vh}{k}\right)}$. Time constants for gating of m and h are given by

$$\tau_{m/h} = \begin{cases} aL + \frac{bL}{1+\exp\left(\frac{-(V-cL)}{dL}\right)} & \text{if } V < VBrk \\ aR + \frac{bR}{1+\exp\left(\frac{V-cR}{dR}\right)} & \text{if } V \geq VBrk \end{cases}.$$